Room temperature infrared detectors made of PbTe/CdTe multilayer composite

S. Chusnutdinow[1, a)], S. Schreyeck[2], S. Kret[1], A. Kazakov[3], and G Karczewski[1]

[1]*Institute of Physics, Polish Academy of Sciences, Al. Lotników 32/46, PL-02-668 Warszawa, Poland*

[2]*Physikalisches Institut, Experimentelle Physik III, Universität Würzburg, D-97074 Würzburg, Germany*

[3]*International Research Center MagTop, Institute of Physics, Polish Academy of Sciences, Al. Lotników 32/46, PL-02-668 Warszawa, Poland*

[a)]Author to whom correspondence should be addressed: chusnut@ifpan.edu.pl

Abstract

We report on fabrication and characterization of infrared detectors made of a composite material – PbTe/CdTe multilayer. The multilayer consists of 10 repetitions of 35 nm thick PbTe layers and 75 nm thick CdTe layers grown by molecular beam epitaxy on GaAs (100) semi-insulating substrates. Simple technological methods were used to manufacture photoresistors from the structure containing the PbTe/CdTe composite. The front-side illuminated photodetectors show a cut-off wavelength of 3.57 μm and a peak current responsivity of 127 mA/W at 10 V bias voltage, frequency 730 Hz and temperature 300 K. The specific detectivity of photoresistors at the peak wavelength of 2.9 μm equals to 2.7×10^{10} cm·Hz$^{1/2}$/W and 6.1×10^{9} cm·Hz$^{1/2}$/W for 77 and 300 K, respectively. Although the SL photoresistors were not optimized, neither antireflection coated nor lithographically defined, their detectivity, especially at room temperature, is high - comparable to that of photoconducting infrared detectors available on the market. Possible mechanisms causing the relatively high performance of PbTe/CdTe SL detectors have been discussed in details. These are a decrease of the electron concentration in the conducting PbTe layers caused by capturing of some mobile electrons by dangling bonds present at the PbTe/CdTe interfaces and the effective suppression of the Auger recombination in nanostructures made of narrow and wide bandgap semiconductors.

Infrared radiation (IR) detectors are widely used in medical, security, military, and commercial applications for various purposes, such as chemical gas analysis, gas leak detection, infrared imaging, remote temperature measurements, etc. In particular, there is a constant interest in applications, and thus the development of IR detectors operating at room temperatures[1-4]. The main purpose of this work is to present a material that is a very promising candidate for highly sensitive room temperature infrared detectors. This material is a composite consisting of PbTe and CdTe layers of nanometric thicknesses forming a PbTe/CdTe multilayer . The PbTe/CdTe composite exhibits different properties than those of component materials, in particular, of thin PbTe layers. For instance, electron concentration in PbTe layers embedded in CdTe is at least by one order of magnitude lower than in pure PbTe. The modified properties make PbTe/CdTe SL detectors highly sensitive to IR radiation even at room temperature.

The idea of constructing IR detectors from a combination of narrow and wide bandgap semiconductors is not new. It is based on observations that photosensitivity of IR detectors made of pure narrow bandgap materials (including PbTe and its solid solution with SnTe), is strongly limited by recombination processes of photo-excited carriers, in particular, by the Auger recombination. On the other hand, in wide bandgap materials, such as GaAs[5] or CdTe[6], the much weaker Auger recombination plays a negligible role. In consequence, it has been experimentally proven that the Auger recombination can be significantly suppressed when the IR detectors are made of a combination of narrow and wide bandgap semiconductors. The effect was demonstrated for such material systems as InAs/$Ga_xIn_{1-x}Sb$[7], HgTe/CdTe[8], $Hg_xCd_{1-x}Te$/CdTe[9], PbSe/CdS[10] and recently PbSe/CdTe[11]. The effective reduction of the Auger recombination in PbSe/CdS and PbSe/CdTe devices results in a measurable spectral photoresponse up to room temperature even when the IR sensitive single PbSe layer was very thin[10,11].

Quantum structures made of a combination of PbTe and CdTe are have been studied for some time. They exhibit unique and interesting features. First of all, the constituents are almost complete immiscible. The immiscibility is a consequence of the fact that although PbTe and CdTe crystallize in cubic crystal structures and have almost identical lattice constants (0.646 and 0.648 nm, respectively), their crystal structures are completely different. In the case of PbTe, it is the rock-salt structure and the zinc-blende structure in the case of CdTe. Because of the immiscibility, both materials are unable to form an alloy. In a solid solution, they tend to separate and form single-phase regions of pure PbTe and CdTe with atomic-scale sharp interfaces between them. The lattice type mismatch results in numerous

broken bonds located at the PbTe/CdTe interfaces. The immiscibility has been used for the spontaneous creation of high-quality PbTe quantum dots (QDs) and quantum wells (QWs) embedded in the CdTe matrix[12-17]. A similar growth mechanism has been employed to form CdTe antidots embedded in conducting PbTe layers. Such structures are important for photoelectric applications[18,19]. Morphology and thermally activated morphological transformations of PbTe/CdTe multilayers were discussed in details in publications[20-22].

The next important property of the PbTe/CdTe material system is a large difference of energy gaps (E_g^{PbTe}=0.32eV; E_g^{CdTe}=1.59eV), as well as, type I band ordering, as confirmed by x-ray photoemission spectroscopy[23]. Thus, background and photoexcited carriers are strongly localized and confined in low-dimensional PbTe objects. This leads to an effective IR luminescence from PbTe/CdTe QDs and QWs[17-20]. The introduction of an array of such PbTe QDs into a depletion layer of a CdTe p-n junction resulted in the first demonstration of infrared electroluminescence at room temperature[24].

In contrary to optical properties, transport properties of PbTe/CdTe quantum wells and superlattices were not systematically studied so far. This is because electron concentration in single PbTe/CdTe QWs appears to be surprisingly low, as will be shown below. At room temperature typical electron carrier concentration in nominally undoped, bulk PbTe is in the order of 10^{18}-10^{19} cm^{-3}. In single PbTe layers embedded in CdTe, it decreases by orders of magnitude and depends on the PbTe layer thickness. In addition, the carrier concentration exponentially decreases with decreasing temperature making low-temperature transport measurements very difficult. The reduction of the carrier concentration and its dependence on temperature is probably caused by the capture of mobile carriers by dangling bonds located at the PbTe/CdTe interfaces.

The investigated samples containing PbTe/CdTe multilayers were grown by molecular beam epitaxy (MBE) on semi-insulating GaAs (100) substrates. The molecular fluxes of elemental Pb, Cd, Te, and Zn were supplied from standard effusion cells. The CdTe layers were deposited in a slight overpressure of Cd with beam equivalent pressures (BEP) for Cd and Te of $1.1x10^{-6}$ and $1.0x10^{-6}$ mbar, respectively. On the other hand, the growth of PbTe requires Te rich conditions, so the BEP for Pb was kept at the value of $6.0x10^{-7}$ mbar. The MBE process was monitored *in situ* by reflection high energy electron diffraction (RHEED), revealing sharp streaky patterns throughout entire growth, indicating good quality structures. After thermal removal of the oxide layer protecting the GaAs (100) surface and cooling the substrate in Zn flux to the growth temperature, the Te shutter was opened for 30 s to deposit about 5 nm of ZnTe. The ultra-thin ZnTe buffer layer is necessary to reduce a huge lattice

mismatch between GaAs and CdTe (13.6%) and to stabilize the further growth in the (100) orientation. In the next 1800 s, 237 nm of CdTe was deposited. The main part of the samples was a SL consisting of several repetitions of PbTe and CdTe layers. The SL was finally capped by a 190 nm of CdTe. After the growth was finished, samples were immediately cooled to room temperature. Samples with various numbers of repetitions and various thicknesses of PbTe and CdTe layers were grown and studied. The applied fluxes and the substrate temperature of 290 C result in the growth rate of 0.183 and 0.132 nm/s for PbTe and CdTe, respectively. Since the various samples show qualitatively similar results, this report is focused on the structure with 10 repetitions of 33 nm PbTe and 72 nm CdTe.

Before characterization by Transmission Electron Microscopy (TEM), the SL structure was annealed for 10 min in the air at the temperature of 200 C to ensure that it is identical to structures those used for optical measurements. The characterization by TEM was performed with the FEI Titan Cube 80-300 microscope operating at 300 kV. For TEM investigation, the electron transparent cross-section was prepared by the Focused Ion beam technique (FIB). This process was performed using Helios Nanloab 600 dual-beam scanning microscope. Prior cutting the protective 50 nm thick Pt-C layer was deposited from metalorganic source using electrons and followed by a thicker layer about 1 µm thick with assistance Ge ion focused beam. Final thinning of lamela was done with Ga ion accelerate by 2kV potential. The element sensitive STEM images was obtained using High Angle Angular Detector (HAADF) with collecting angle of the scattered electron in the range of 80 - 200 mrad. Figure 1a shows an overview of a 6 µm long fragment of the SL heterostructure taken by STEM-HAADF at low magnification. The period of SL calculated from STEM images is 106.5 +/- 0.8 nm, and it is constant in the field of view. Figure 1b reveals the PbTe quantum wells are covered by pairs of small, pyramidal structures which are located opposite one to each other on both sides of CdTe barriers. No threading dislocations or stacking faults propagating to the SL are visible in the ZnTe/CdTe buffer layer, which indicates that this kind of buffer is very effective. High resolution STEM image presented in Figs. 1c shows that the CdTe/PbTe interface is are atomically flat at the scale of tens nanometers contrary to the PbTe/CdTe interface where the atomic layer discontinuities, indicated by red arrows, are clearly visible. Broken atomic bonds at the atomic layer discontinuities can effectively trap free electrons from the PbTe quantum wells, thus decreasing their concentration.

The SL structure shown in Figure 1 was used to manufacture simple resistors. Firstly, 1×3 mm^2 bars were cleaved from the as-grown wafer. To provide electrical contacts at both ends of the indium bars was soldered to the topmost CdTe cap layer. Subsequently, the bars

with In contacts were annealed at 200 C for 10 min in an air atmosphere. The annealing results not only in PbTe/CdTe intermixing shown in Fig.1b, but also it enhances diffusion of In into the bulk of the samples, thus ensuring good electrical contacts to all 10 PbTe layers at entire SL thickness.

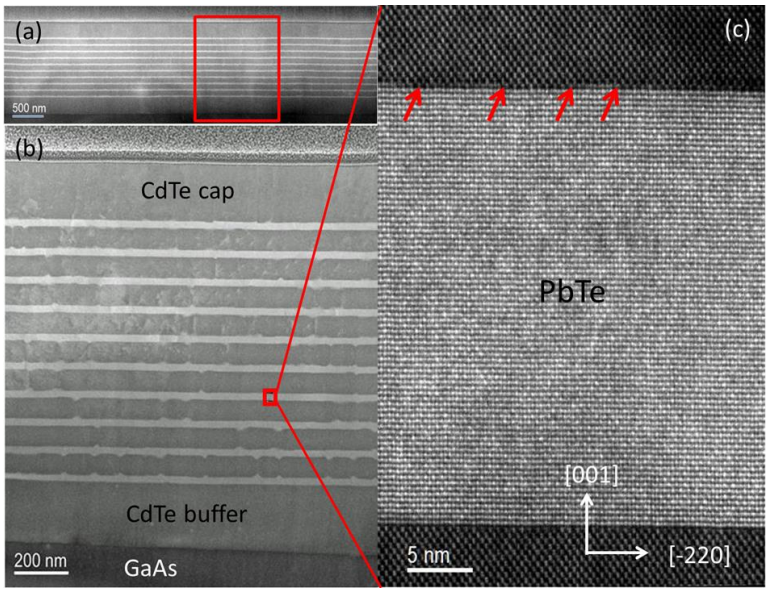

Fig.1. Transmission electron microscope (TEM) images of the PbTe/CdTe multilayer structure. Prior to TEM measurements the as-grown structure was annealed in air at 200 C for 10 min. a) STEM-HAADF image of 6 µm long fragment of CdTe/PbTe SL; b) enlarged fragment of the SL with the width corresponding to the frame in figure a; c) HR-STEM image of one PbTe layer with the width corresponding to the frame in figure b, arrows point the atomic monolayer discontinuities at PbTe/CdTe interface.

The photoelectric response of the resistors to infrared radiation was measured in a wide spectral range by using an infrared spectrometer consisting of a M150 Solar Laser System monochromator, a Newport 6363 IR light source and a Thorlabs mechanical chopper with variable chopping frequency. The resistors were biased with a dc bias voltage up to 10 V. The photoinduced alternating current (AC) was amplified by a Femto Low Noise Current Amplifier DLPCA-200 and measured by a Zurich Instruments MLFI 5MHz lock-in amplifier. The measurements were carried out in the temperature range 77-300 K and in the frequency range 90-730 Hz. The MLFI lock-in amplifier was used for measurements of noise power spectral density, which is needed for calculations of detectivity of the SL resistors.

The spectral responsivity, $R_i(\lambda)$, of photoresistive sensors, defined as the ratio of the photocurrent $I_{ph}(\lambda)$ to the optical power $P_{op}(\lambda)$ hitting the active area of the device, is given by the relation:

$$R_i = I_{ph}(\lambda)/P_{op}(\lambda), \text{[A/W]} \qquad (1)$$

Figure 2 shows responsivity spectra, $R_i(\lambda)$, of a PbTe/CdTe SL photoresistor measured in the spectral region 1.5 - 4.5 μm at various temperatures from 77 to 300 K. The current responsivity, $R_i(\lambda)$, is proportional to the dc bias voltage and it increases with the increasing chopper frequency, the spectra shown in Fig 2 were taken at the highest bias and highest frequency available in our experimental setup, 10 V and 730 Hz, respectively. Except of the very strong H_2O absorption band at 2.73 μm, in a wide spectral range from 1.75 to 3.25 μm, the responsivity is almost constant, what indicates that the detector is flat. The shape of $R_i(\lambda)$ changes very little with temperature, except for the long-wavelength edge, which flattens as the temperature decreases. This flattening reflects the red-shift of the responsivity cut-off wavelength, which is due by decreasing of the PbTe bandgap with decreasing temperature.

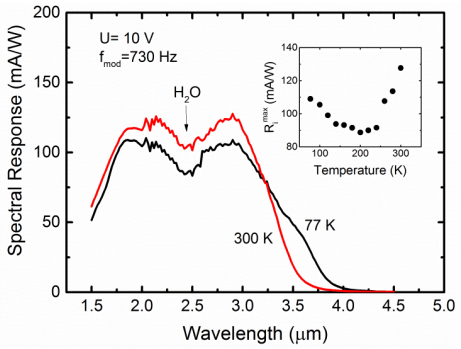

Fig. 2. The current spectral Response, $R_i(\lambda)$, as a function of wavelength taken at 300 and 77 K. The measurements were carried out at 10 V dc bias and 730 Hz frequency. In the inset, the temperature dependence of the peak current responsivity, R_i^{max}, at λ=2.9 μm.

The peak current responsivity, R_i^{max}, of this device appears at the wavelength of 2.9 μm and equals to 127 mA/W at 300 K. In order to illustrate the temperature dependence of the responsivity, in the inset to Fig. 2 the temperature behavior of the peak responsivity R_i^{max} is shown. It is worth notice that the responsivity signal is the strongest at room temperature. It decreases with the decreasing temperature reaching a minimum at about 200 K and increases again at $T < 200$ K. This is quite surprising since the responsivity of narrow bandgap detectors usually strongly increases with the decreasing temperature reaching the highest

values around the LN_2 temperature. The unusual temperature dependence of responsivity resembles the temperature dependence of the Auger recombination limited lifetime of photoexcited carriers in bulk PbTe[25]. This may suggest that the responsivity of PbTe/CdTe SL photoresistor is also limited by Auger recombination, as expected.

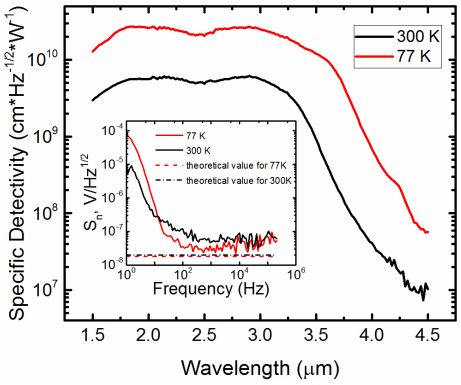

Fig. 3. Spectral dependencies of specific detectivity and noise density (in the inset) at 77 and 300 K. The broken lines in the inset represent the theoretical values of thermal noise densities at 77 and 300 K.

Having measured the responsivity spectra, $R_i(\lambda)$, one can calculate an external quantum efficiency of the photoresistor by the equation[1]:

$$\eta = R_i(\lambda)E_\lambda/q, \qquad (2)$$

where E_λ, is the photon energy of detected light, and q is the electron charge. Substituting the measured values of responsivity in Eq. (2), one obtains quantum efficiency values of 7 and 5% for 2.0 and 2.9 μm, respectively. The low values of the external quantum efficiency results, at least in part, from a very strong reflection of IR radiation from the SL structure due to the very large refractive index of PbTe, approaching n = 6 around λ=3 μm.

The specific detectivity of the photoresistor, D^*, plotted in Fig. 3, is calculated by the well-known relation:

$$D^* = \frac{R_i R\sqrt{A\Delta f}}{V_n} = \frac{R_i R\sqrt{A}}{S_n}, \ [\text{cm} \times \text{Hz}^{1/2}/\text{W}] \qquad (3)$$

where A=0.01 cm^2 is the photosensitive surface area of the detector, R_i is spectral responsivity expressed A/W, Δf is the frequency bandwidth, S_n is noise spectral density expressed in units of $V/Hz^{1/2}$, R is the resistance of the structure. The resistance of the device, R, was determined from I-V characteristics measured at various temperatures. At high temperatures (T>240 K)

the I-V curves are perfectly linear in entire bias range from -10 to +10 V. At lower temperatures the linearity holds only for lower bias (-8V<V<+8V). For higher voltages the I-V characteristics incline from straight line indicating that the resistance of the device slightly increases with increasing bias. Nevertheless for calculation of D* we took the resistance at zero bias according to the formula $R=(dV/dI)_{V=0}$. Such procedure resulted in resistance values of 24 and 78 kΩ for 300 and 77 K, respectively. The noise spectral density, S_n, measured at 300 and 77 K is shown in the inset to Fig. 3. As expected, for low frequencies, S_n strongly decreases with increasing frequency, and around 0.5-1.0 kHz reaches a minimum. At 730 Hz, the noise density is 50.3 and 31.5 nV/Hz$^{1/2}$ at 300 K and 77K, respectively. These values exceed the theoretical values of the thermal noise density, the dominant noise source in resistors, by a factor of 3. However, the measured noise density in the SL resistor is not large, which indicates the good quality of the electrical contacts. In consequence, the specific detectivity of the photoresistor, D^* at the wavelength of 2.9 µm, equals to 6.1×10^9 and 2.7×10^{10} cm·Hz$^{1/2}$/W at 300 and 77K, respectively. In view of the fact that the noise spectral density does not depend on the radiation wavelength, it is obvious that the detectivity spectrum, $D^*(\lambda)$, shown in Fig. 3, has the same shape as the spectral responsivity $R_i(\lambda)$, shown in Fig. 2.

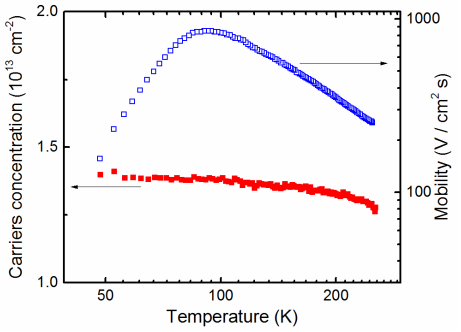

Fig.4. Electron carrier concentration and electron mobility of the PbTe/CdTe multilayer structure.

It is noteworthy that, despite the low spectral responsivity and external quantum efficiency, detectivity, especially detectivity at room temperature, is relatively high. It is comparable with detectivity of other IR detectors operating at room temperatures, particularly those commercially available. For instance, detectivity of the PC-4 CdHgTe photoconductive detector with the cut-off wavelength of 3.8 µm produced by Vigo System Ltd. is

$3x10^9$ cm·$Hz^{1/2}$/W at 300 K and increases to $3x10^{10}$ cm·$Hz^{1/2}$/W at 230 K[26]. Photoconductive InSb detectors offered by Hamamatsu (P6606) exhibit very similar detectivities; however, their peak sensitivity occurs at longer wavelengths, 4-6 μm[27].

In order to explain the relatively high detectivity of the PbTe/CdTe SL, electron concentration and mobility were measured in a function of temperature. For transport measurements the samples were cleaved to the form of 2 × 6 mm rectangles. Six Indium contacts in a Hall bar-like configuration were soldered from the top. A standard, low-frequency lock-in technique was applied for the resistance measurements. As shown in Fig. 4, above 100 K the SL exhibits a metallic-like conductivity with almost temperature-independent carrier concentration high mobility of carriers. Taking into account the total thickness of the 10 PbTe conducting channels forming the SL, 350 nm, the resulting three-dimensional electron concentration equals to about $3x10^{17}$ cm^{-3}. It is, thus, at least one order of magnitude lower than in the case of undoped, bulk PbTe samples. The decrease of the number of free electrons is probably caused by capturing them by dangling bonds which are present at the PbTe/CdTe interfaces. Since the dielectric constant of PbTe is large (appr.1000) and the conducting PbTe channels are thick (33 nm), potential fluctuations originating from the charges captured at interfaces are effectively screened. The screening prevents scattering of free electrons located in the center of the PbTe layers and assures their high mobility, even at high temperatures. We are convinced that the observed high detectivity of PbTe/CdTe SL photoresistors results from the reduced concentration of highly mobile electrons and the reduced the Auger recombination in this kind of heterostructures.

In summary, we have shown that PbTe/CdTe multilayers are an attractive material for the production of infrared radiation detectors. The photoresistors are containing the SLs exhibit relatively high detectivities even at the room temperature. Optimizing the SL design, using antireflection coating, and using lithography to define the active area is likely to further increase detection performance.

Acknowledgments

The research in Poland was partially supported by the National Science Centre through Grants No.2017/25/B/ST3/02966 and 2018/30/M/ST3/00276 and by the Foundation for Polish Science through the IRA Program co-financed by the European Union within SGOP and in Germany by the DFG through the SFB 1170 "ToCoTronics" (project No. A05).

PLEASE CITE THIS ARTICLE AS DOI: 10.1063/5.0018686

Data Statement

The data that support the findings of this study are available from the corresponding author upon reasonable request

References

1. A. Rogalski, Prog Quant Electron **27**, 59-210 (2003).

2. A. Rogalski, Infrared Physics & Technology **54**, 136-154 (2011).

3. A. Rogalski, *Infrared Detectors, Second Edition*. (CRC Press, 2010).

4. A. Rogalski, *Infrared and Terahertz Detectors*. (CRC Press, 2019).

5. G. W. Charache, P. F. Baldasaro, L. R. Danielson, D. M. DePoy, M. J. Freeman, C. a. Wang, H. K. Choi, D. Z. Garbuzov, R. U. Martinelli, V. Khalfin, S. Saroop, J. M. Borrego and R. J. Gutmann, Journal of Applied Physics **85**, 2247-2252 (1999).

6. R. T. Williams, J. Q. Grim, Q. Li, K. B. Ucer, G. A. Bizarri and A. Burger, in *Excitonic and Photonic Processes in Materials*, edited by J. Singh and R. T. Williams (Springer Singapore, Singapore, 2015), pp. 299-358.

7. J. R. Meyer, C. L. Felix, W. W. Bewley, I. Vurgaftman, E. H. Aifer, L. J. Olafsen, J. R. Lindle, C. A. Hoffman, M. J. Yang, B. R. Bennett, B. V. Shanabrook, H. Lee, C. H. Lin, S. S. Pei and R. H. Miles, Applied Physics Letters **73**, 2857-2857 (1998).

8. I. Vurgaftman, J. R. Meyer, J. M. Dell, T. A. Fisher and L. Faraone, Journal of Applied Physics **83**, 4286-4286 (1998).

9. Y. Jiang, M. C. Teich and W. I. Wang, Journal of Applied Physics **69**, 6869-6875 (1991).

10. B. B. Weng, J. J. Qiu, L. H. Zhao, C. Chang and Z. S. Shi, Applied Physics Letters **104,** 121111 (2014).

11. S. Chusnutdinow, M. Szot, T. Wojtowicz and G. Karczewski, AIP Advances **7**, 035111 (2017).

12. W. Heiss, H. Groiss, E. Kaufmann, G. Hesser, M. Booberl, G. Springholz, F. Schaffler, K. Koike, H. Harada and M. Yano, Applied Physics Letters **88**, 192109 (2006).

13. R. Leitsmann, L. E. Ramos and F. Bechstedt, Phys Rev B **74**, 085309 (2006).

14. K. Koike, T. Honden, I. Makabe, F. P. Yan and M. Yano, Journal of Crystal Growth **257**, 212-217 (2003).

15. H. Groiss, E. Kaufmann, G. Springholz, T. Schwarzl, G. Hesser, F. Schaffler, W. Heiss, K. Koike, T. Itakura, T. Hotei, M. Yano and T. Wojtowicz, Applied Physics Letters **91**, 222106 (2007).

16. T. Schwarzl, E. Kaufmann, G. Springholz, K. Koike, T. Hotei, M. Yano and W. Heiss, Phys Rev B **78**, 165320 (2008).

17. R. Leitsmann and F. Bechstedt, Phys Rev B **80**, 165402 (2009).

18. M. Szot, K. Dybko, P. Dziawa, L. Kowalczyk, E. Smajek, V. Domukhovski, B. Taliashvili, P. Dluzewski, A. Reszka, B. J. Kowalski, M. Wiater, T. Wojtowicz and T. Story, Crystal Growth & Design **11**, 4794-4801 (2011).

19. Y. Z. Pei, A. D. LaLonde, N. A. Heinz and G. J. Snyder, Adv Energy Mater **2**, 670-675 (2012).

20. G. Karczewski, M. Szot, S. Kret, L. Kowalczyk, S. Chusnutdinow, T. Wojtowicz, S. Schreyeck, K. Brunner, C. Schumacher and L. W. Molenkamp, Nanotechnology **26**, 135601 (2015).

21. M. Mińkowski, M. A. Załuska-Kotur, Ł. A. Turski and G. Karczewski, Journal of Applied Physics **120**, 124305 (2016).

22. M. Mińkowski, M. A. Załuska-Kotur, S. Kret, S. Chusnutdinow, S. Schreyeck, K. Brunner, L. W. Molenkamp and G. Karczewski, Journal of Alloys and Compounds **747**, 809-814 (2018).

23. J. Si, S. Jin, H. Zhang, P. Zhu, D. Qiu and H. Wu, Applied Physics Letters **93**, 202101 (2008).

24. A. Hochreiner, T. Schwarzl, M. Eibelhuber, W. Heiss, G. Springholz, V. Kolkovsky, G. Karczewski and T. Wojtowicz, Applied Physics Letters **98**, 021106 (2011).

25. K. Lischka, Applied Physics a-Materials Science & Processing **29**, 177-189 (1982).

26. www.vigo.com.pl.

27. www.hamamatsu.com/eu/en/product/type/P6606-310/index.html.

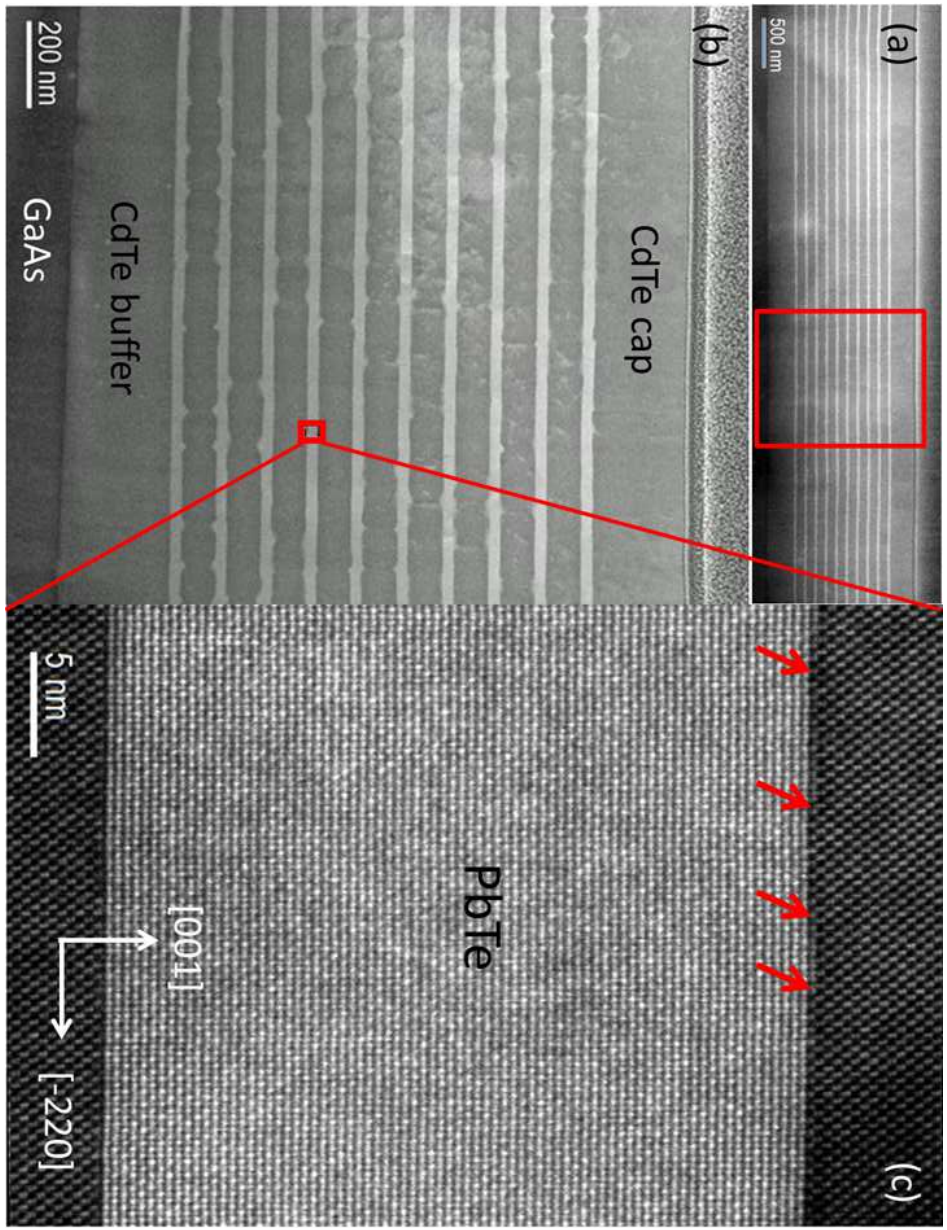

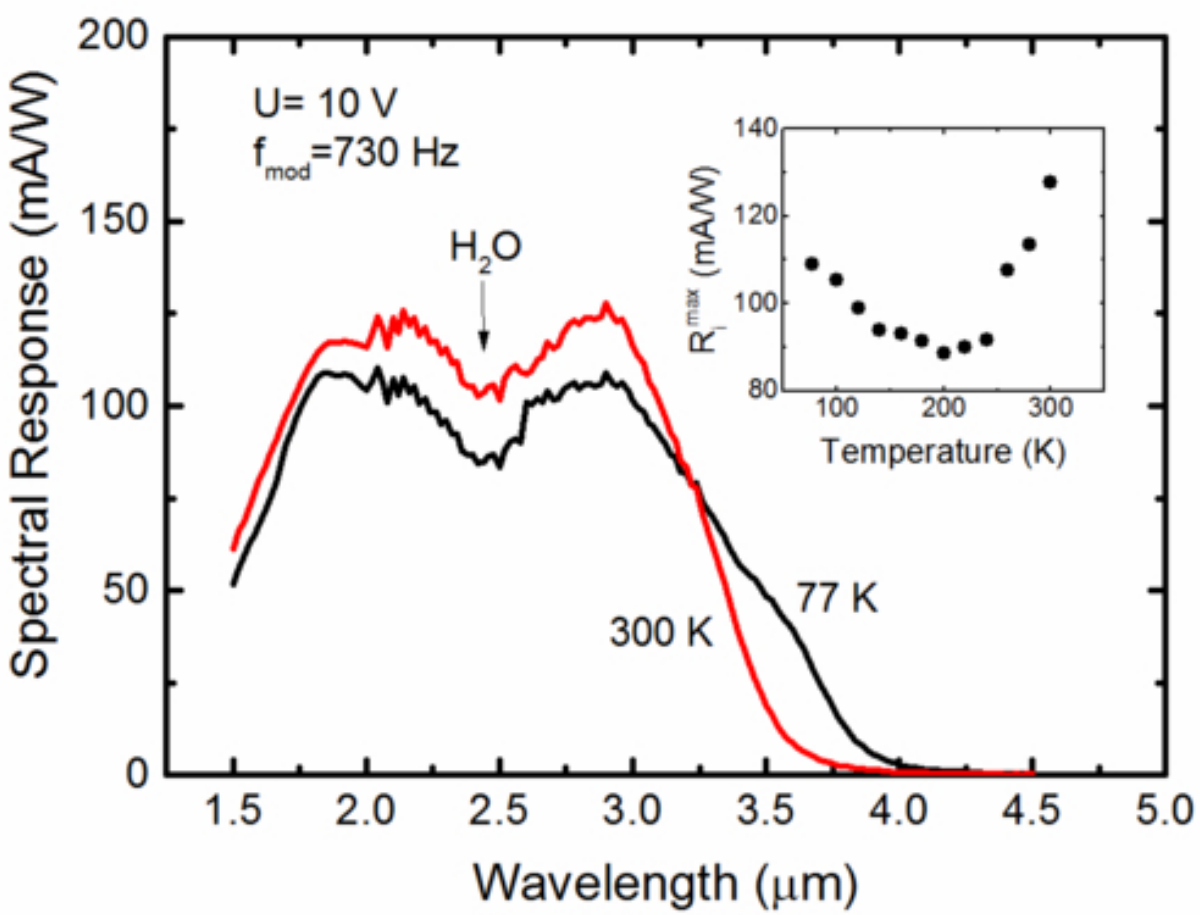

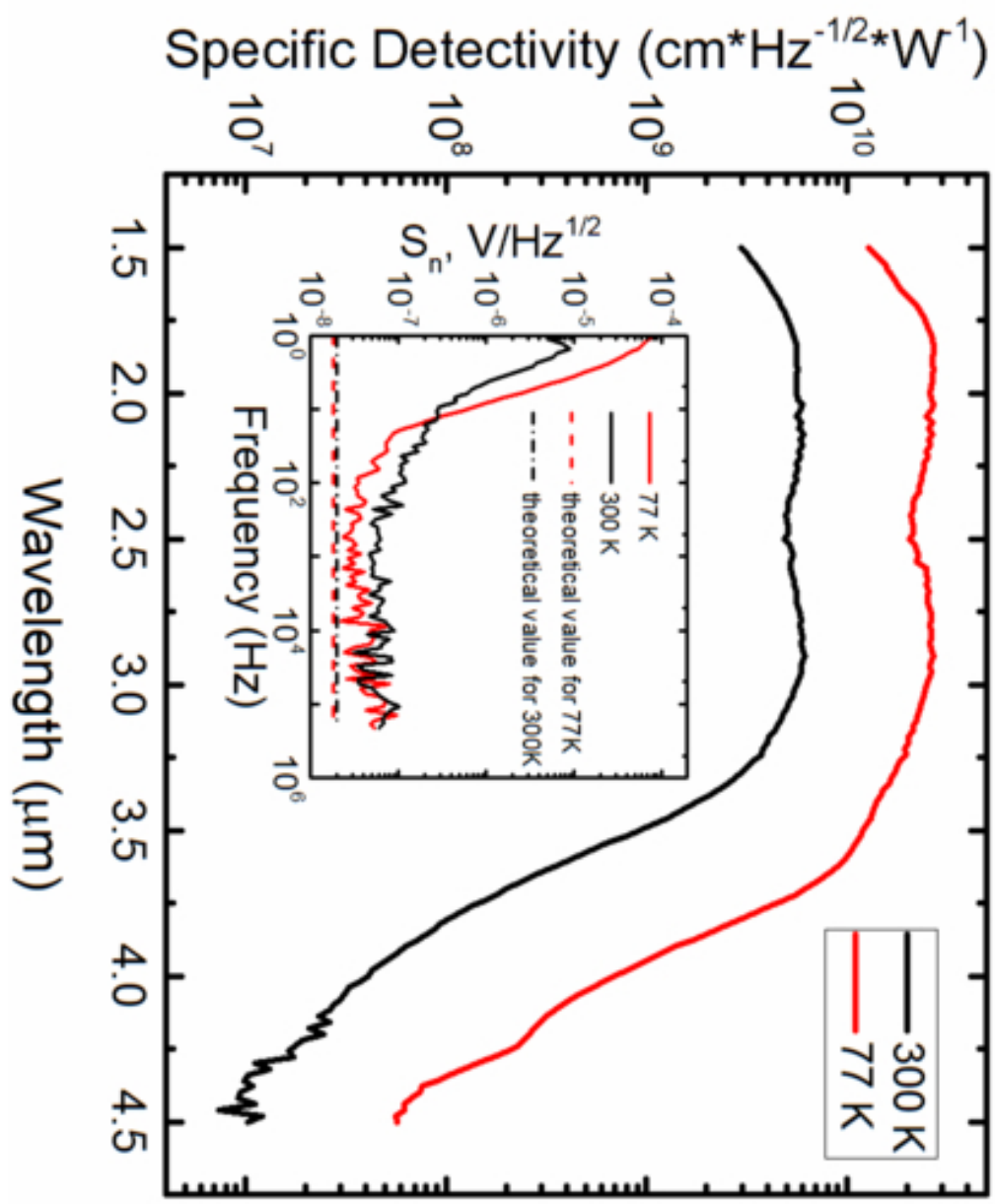

PLEASE CITE THIS ARTICLE AS DOI: 10.1063/5.0018686